Available online at www.sciencedirect.com

SciVerse ScienceDirect

Ceramics International 39 (2013) 8237–8243

CERAMICS INTERNATIONAL

www.elsevier.com/locate/ceramint

Effect of Co_3O_4 content and compaction pressure on the microstructure and electric properties of SnO_2–Sb_2O_5–Cr_2O_3 varistor ceramics

J.A. Aguilar-Martínez[a,*], M.I. Pech-Canul[b], César Leyva-Porras[a], Edén Rodríguez[c], V. Iván Hernández[d]

[a]Centro de Investigación en Materiales Avanzados, S.C. (CIMAV), Alianza Norte No. 202, Parque de Investigación e Innovación Tecnológica (PIIT), Nueva Carretera Aeropuerto km. 10 C.P., 66600 Apodaca Nuevo León, Mexico

[b]Centro de Investigación y de Estudios Avanzados del IPN Unidad Saltillo, Carretera Saltillo-Monterrey Km. 13.5, Ramos Arizpe Coahuila, 25900, Mexico

[c]Facultad de Ingeniería Mecánica y Eléctrica, Universidad Autónoma de Nuevo León, San Nicolás de los Garza, Nuevo León, Mexico

[d]KEMET, Antiguo camino al Mezquital #100, San Nicolás de los Garza, N.L. 66490, Mexico

Received 26 February 2013; received in revised form 2 April 2013; accepted 2 April 2013
Available online 8 April 2013

Abstract: The effect of Co_3O_4 content (1 and 5 mol%) and powder compaction pressure (55, 110, and 166 MPa) on the microstructure and nonlinear electrical behavior of SnO_2-based ceramics prepared by high-energy milling was investigated. The results show a correlation between the compaction pressure and Co_3O_4 content with the electrical properties. At constant oxide concentration and with increase in the compaction pressure, there is a slight decrease in the breakdown electric field and an increase in the nonlinearity coefficient. Conversely, at the highest Co_3O_4 content the breakdown electric field varies slightly, whilst the nonlinearity coefficient is maintained to be constant. A decrease in grain size with Co_3O_4 increase is ascribed to the formation of the cobalt/tin oxide spinel (Co_2SnO_4) at the grain boundaries. The best electrical characteristics were achieved with 1 mol% Co_3O_4 and 166 MPa, that is, nonlinear coefficient of 13.24 and breakdown electric field of 830 V/cm. Based on thermal analyses, possible reactions for Co_2SnO_4 formation are outlined.

Keywords: B. Grain boundaries; B. Grain size; C. Electrical properties; D. Ceramics; E. Varistors

1. Introduction

Varistors are ceramic semiconductor devices with highly nonlinear current–voltage characteristics. These materials are commonly used as over-voltage and surge absorbers in electronic circuits and electrical systems [1,2]. The current–voltage ($j(E)$) characteristic of varistor ceramics is frequently approximated by the empirical power-law relation

$$j = kE^{\alpha}, \tag{1}$$

where j is the current density and E is the average electric field; k and α are constants. The degree of the nonlinearity of current–voltage characteristic is estimated by the nonlinearity coefficient

$$\alpha = \frac{\rho_s}{\rho_d} = \frac{E}{j}\frac{dj}{dE} = \frac{d(\ln j)}{d(\ln E)}, \tag{2}$$

giving the ratio of the static resistivity $\rho_s = E/j$ to the differential resistivity $\rho_d = dE/dj$at a fixed current density, where nonlinearity is high. The integration of Eq. (2) with the condition α=const gives the expression (1). The nonlinearity coefficient α and the electric field strength E are considered to be the main parameters of varistor ceramics. The greater the value of α, the better the device.

Tin dioxide (SnO_2) is an n-type semiconductor with a rutile-type structure and space group D_{4h}^{14} [$P4_2/mnm$] [3]. Tin dioxide exhibits interesting physical properties suitable for various applications [3–5]. The processing of SnO_2-based material with high density allows it to be considered as a promising material in other types of electronic devices such as varistors [6]. An adverse fact that restricts the application of this oxide is its low densification rate during sintering because of

*Corresponding author. Tel.: +52 81 11560805; fax: +52 81 11560820.
E-mail addresses: josue.aguilar@cimav.edu.mx, jaguilar_mtz@hotmail.com (J.A. Aguilar-Martínez).

0272-8842/$ - see front matter © 2013 Elsevier Ltd and Techna Group S.r.l. All rights reserved.
http://dx.doi.org/10.1016/j.ceramint.2013.04.008

the predominance of non-densifying mechanisms for mass transport, such as surface diffusion (at low temperatures) and evaporation–condensation (at high temperatures) which promote only pure coarsening and grain growth [7]. However, tin dioxide dense ceramics can be obtained by the introduction of densifying agents, such as CoO among others [8–12] or by hot isostatic pressure processing [13], which promote the densification of SnO_2 almost to the theoretical density value. In a previous work it has been reported that 1.0 mol% CoO is the most favorable dopant content for addition to obtain dense SnO_2-based ceramic materials [8].

However, there are other key processing parameters, such as the compaction pressure, that impact the densification of ceramic powders and, consequently, the electrical properties and mechanical behavior. During processing, the pressing stage is important because it affects the powder distribution within the pellet mold and the pellet's mechanical strength. But also the aim of this stage is to decrease the volume of pores within the sample by reordering or accommodating the grains. Thus, the optimum pressure should be just enough to compact the powder mix into a defined shape that can be handled easily and without causing any cracks. Having the powders in an optimum packing facilitates the next stage on the processing line, the sintering, which promotes sample densification and governs both grain growth and the number of grain boundaries.

Although the pressing stage is considered to be of great importance, investigations that include a systematic study on the effect of compaction pressure on the microstructure and electrical properties of SnO_2-based ceramics are scarce. In the case of Bi-2223 superconductor ceramic materials, it has been found that the critical current under low applied magnetic fields is very sensitive to the compaction pressure [14].

In this work, SnO_2-based ceramics were prepared, and the effect of compaction pressure and Co_3O_4 content on the electrical properties of SnO_2–Cr_2O_3–Sb_2O_5 varistors was investigated. The aim of the addition of 1.0 and 5.0 mol% of Co_3O_4 in this work is to correlate the content of dopant with the varistors electrical properties, rather than the effect on density.

2. Experimental

The raw chemicals used in this work, SnO_2 (Baker), Co_3O_4 (Baker), Sb_2O_5 (Aldrich) and Cr_2O_3 (Baker), were of analytical grades. The molar composition of the investigated systems was 99.87−*X*% SnO_2−*X*% Co_3O_4−0.05% Sb_2O_5−0.08% Cr_2O_3, where $X=1$ and 5 mol%. The powders were processed by a non-conventional method of mixture, through high-energy milling performed for 20 min in a planetary ball-mill (Pulverisette 7, Fritsch GmbH) using vials and balls of agate.

The resulting powders were uniaxially pressed in the form of tablets (10.0 mm diameter and about 1.2 mm thick) at different pressure values (55, 110, and 166 MPa) without using any kind of binder. The tablets were sintered in ambient atmosphere at 1350 °C for 1 h using a heating and cooling rate of 6 °C/min in a tube furnace (Lindberg/Blue STF55433C-1). The microstructure was characterized by scanning electron microscopy (Hitachi SEM, model S-3500N). The mean grain size was determined from SEM micrographs, using an Image Analysis Software (Image-Pro Plus), according to the ASTM-E112 standard procedures. The presence of ceramic phases was determined by X-ray diffraction (PANalytical XRD, model Empyrean) using CuK_α radiation ($\lambda=1.5406$ Å) operated at 40 kV and 35 mA and an X'Celerator detector in a Bragg–Brentano geometry. The scans were performed in the 2θ range 10–100° with a step scan of 0.016° and 80 s per step in a continuous mode. The incident beam passed through a 0.04 rad soller slit, a (1/2)° divergence slit, a 10 mm fixed mask, and a 1° fixed antiscatter slit. Meanwhile the diffracted beam passed through a 0.04 rad large soller slit, a (1/2)° divergence slit and a beta nickel filter. Structure refinements and phase identification were performed using the X'Pert HighScore Plus software, version 3.0d and ICDD PDF-4 plus database (ICDD-International Centre for Diffraction Data, Newtown Square, PA).

For electrical characterization, silver electrodes were placed on both faces of the sintered ceramic samples followed by thermal treatment at 800 °C for 6 min. Current–voltage measurements were performed using a high voltage measure unit (Keithley 6487).

Rietveld's method was successfully applied for determination of the quantitative phase of all samples. This method is based on the least squares refinement procedure where the experimental step-scanned values are adapted to calculated ones. The profiles are considered to be known, and a model for a crystal structure is available. The weight fraction (*Wi*) for each phase was obtained from the mathematical relationship for refinement

$$W_i = \frac{S_i(ZMV)_i}{\sum_j S_j(ZMV)_j} \tag{3}$$

where i is the value of j for a particular phase among the N phases present, S_j is the refined scale factor, Z is the number of formula units per unit cell, M is the molecular weight of the formula unit and V is the unit cell volume.

The Rietveld refinement has been done by adjusting major parameters like, scale factor, flat background, zero-point shift, lattice parameters, orientation parameters, peak width parameters (U, V, and W), asymmetry parameter and peak shape. Peak profiles were fitted with the pseudo-Voigt function.

The quality of fitting is judged through the minimization of weighted residual error (R_w), through a Marquardt least-square program defined as

$$R_{wp} = \left[\frac{\sum_i w_i(I_o - I_c)^2}{\sum_l w_i I_o^2}\right]^{1/2} \tag{4}$$

The goodness of fit (*GoF*) is established by comparing R_{wp} with the expected error, R_{exp}:

$$R_{exp} = \left[\frac{N-P}{\sum_i w_i I_o^2}\right]^{1/2} \tag{5}$$

where I_o and I_c are the experimental and calculated intensities, respectively, $w_i = 1/I_o$ and N are the weight and number of

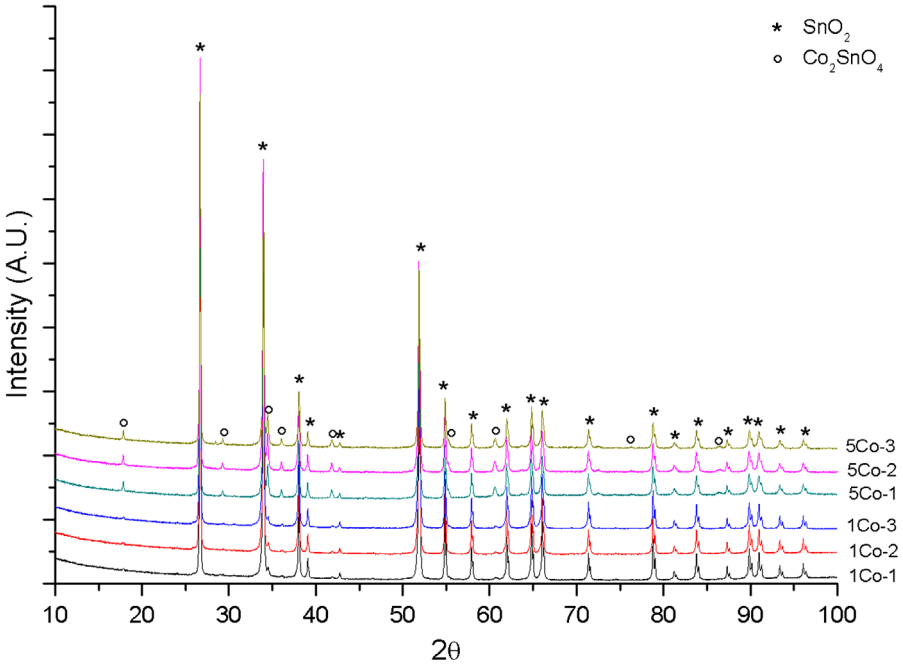

Fig. 1. XRD patterns of specimens with 1 and 5 mol% Co_3O_4, pressed at 55, 110 and 166 MPa (1Co-1, 1Co-2, 1Co-3 and 5Co-1, 5Co-2, 5Co-3, respectively).

experimental observations, and P is the number of fitting parameters i.e. the value of goodness of fit is

$$GoF = \frac{R_{wp}}{R_{exp}} \tag{6}$$

Refinement continues until convergence is reached.

3. Results and discussion

Results from the characterization by XRD and SEM show evidence of cobalt/tin oxide spinel (Co_2SnO_4) formation and its effect on the grain size of the ceramic varistor, respectively. The XRD patterns in Fig. 1 for specimens with 1 and 5 mol% addition of cobalt oxide indicate that in all cases, for samples pressed at 55, 110 and 166 MPa and with 5 mol% Co_3O_4, the spinel phase Co_2SnO_4 is present in addition to the tin oxide (SnO_2) matrix. In the diffractograms, the specimens identified as 5Co-1, 5Co-2 and 5Co-3 correspond to the three levels of compaction pressing, in that order.

On the other hand, the photomicrographs shown in Fig. 2 evidence an overall decrease in grain size when the Co_3O_4 content is augmented from 1 to 5 mol%. In the images, the right-hand photomicrographs correspond to the specimens with the highest level of oxide addition while variation in compaction pressure increases from top to bottom. Although there is no tendency in grain size when the oxide content is fixed and the pressure is varied, a decrease in grain size is observed when the compaction value is maintained constant whilst the oxide content varies from 1 to 5 mol%. Since the spinel is the only new phase in the microstructure, at this point it is assumed to be responsible for the observed results. As for the effect of pressure, interestingly, as shown in Table 1, the highest decrease in grain size is observed with the lowest compaction pressure. A possible explanation for this outcome is that at high compaction pressures, stresses and frictional forces between particles produce a negative effect by impeding transport mechanisms during sintering. Despite the relevance of compaction pressure, only a few works have addressed this issue in the past, essentially dealing with simplified assumptions in the calculation of frictional forces acting during pressing [15]. Therefore, more detailed investigations are required in order to elucidate the effect of compaction pressure.

Current density as a function of electrical field curves measured at room temperature for all samples are shown in Fig. 3. From these graphs it can be noticed that samples doped with 5 mol% Co_3O_4 at different compact pressures have a variation with respect to the breakdown electric field while the nonlinear coefficient values are very similar. On the other hand, the same figure reveals that the samples doped with 1 mol% Co_3O_4 have breakdown electric fields which are significantly lower than those of samples doped with higher Co_3O_4 content. This effect can be noticed objectively in Table 1, which summarizes the values of grain size, nonlinear coefficient (α) and breakdown electric field (E_B) corresponding to specimens where the Co_3O_4 content and compaction pressure were varied.

From Table 1 it can be noticed that the magnitude of E_B for specimens with 5 mol% Co_3O_4 is approximately twice that of the samples with 1 mol% Co_3O_4. Like the grain size observation, this behavior can be ascribed only to the spinel formation, evidenced in the analysis by XRD and phase quantification by Rietveld's method, shown in Table 2. Nonetheless, and in order to support this argument, results from thermal analyses (TG and DSC, thermogravimetric and differential scanning calorimetry) of Co_3O_4 are presented in the next paragraph.

The thermogravimetric curve in Fig. 4(a) shows that upon heating a sample of Co_3O_4, two endothermic events,

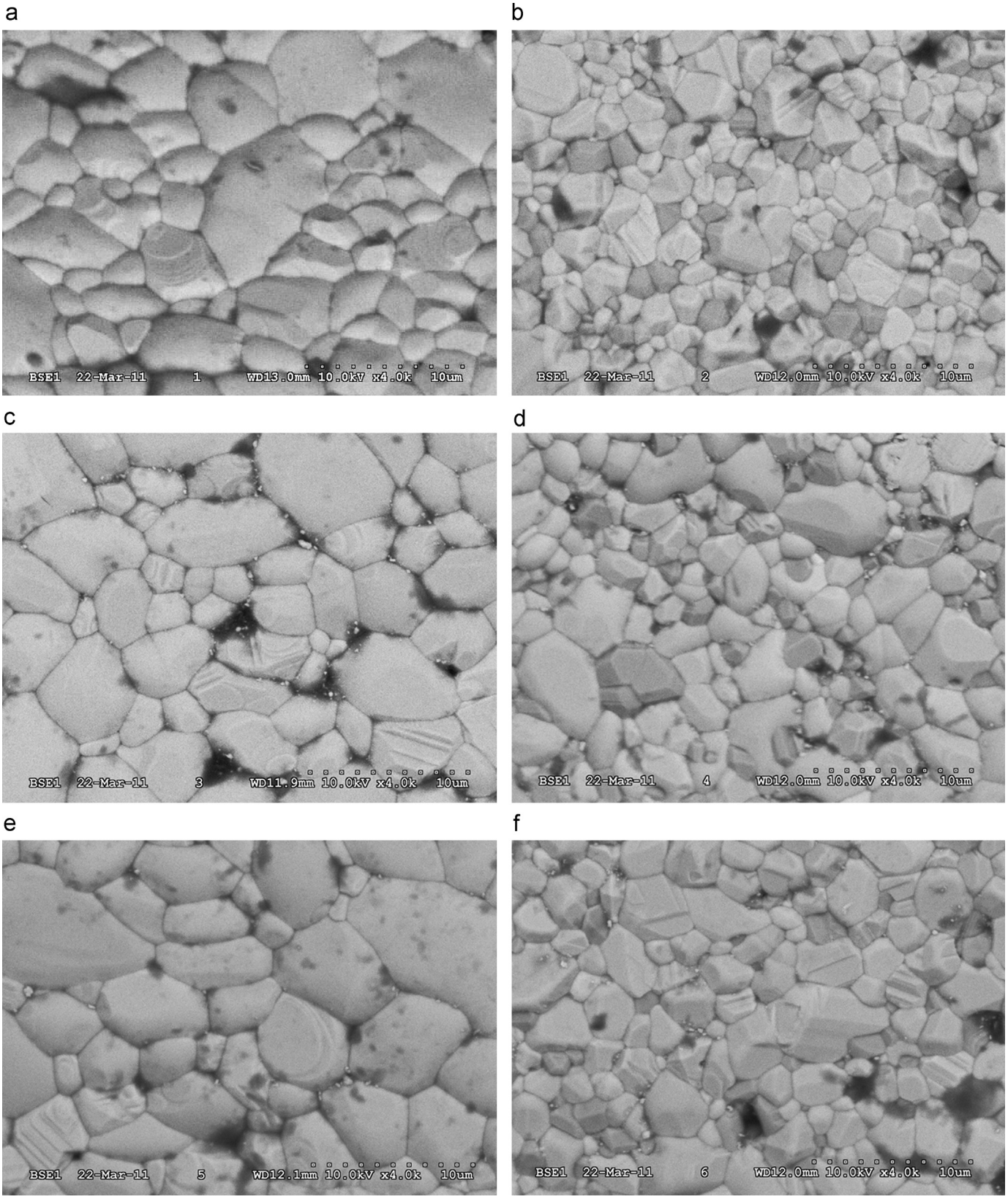

Fig. 2. SEM photomicrographs of specimens with 1 mol% [(a), (c), and (e)] and 5 mol% [(b), (d), and (f)] Co_3O_4, pressed at 55 [(a), (b)], 110 [(c), (d)], and 166 MPa [(e), (f)].

corresponding to weight losses are observed, the first attributed to water evaporation—completed at 400 °C—and the second ascribed to the decomposition of Co_3O_4 into CoO (according to Eq. (7)) exhibiting a maximum at 885 °C. These weight losses are of 0.35% and 6.96%, correspondingly.

$$2Co_3O_4 \overset{850\ ^\circ C}{\rightarrow} 6CoO + O_2(\uparrow) \quad (7)$$

Table 1
Effect of the sintering temperature on the electrical properties and average grain size.

Co_3O_4 (mol%)	Pressing (MPa)	Grain size (μm)	α	E_B (V/cm)
1	55	14.29	10.86	1723.80
5	55	7.82	9.50	3420.18
1	110	12.55	10.66	1504.85
5	110	9.11	9.53	3180.95
1	166	14.2	13.24	829.96
5	166	8.5	9.88	3227.72

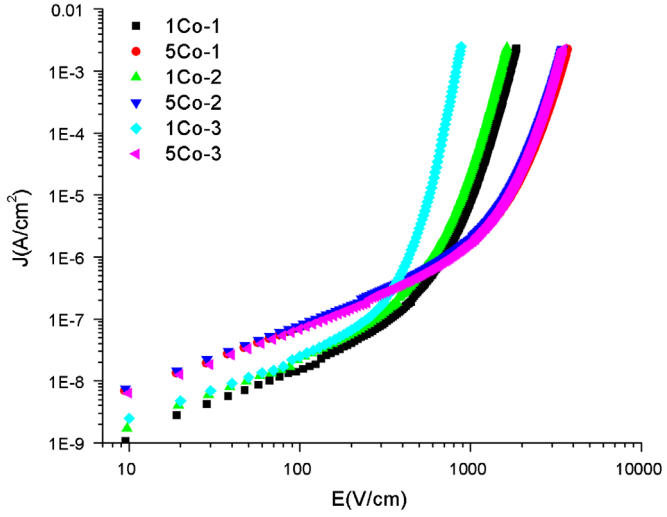

Fig. 3. *J–E* characteristic plots for all samples.

Consecutively and in a separate test, stoichiometric amounts of reagent grade SnO_2 and Co_3O_4 to produce 100% spinel were mixed and analyzed by TG/DTA. The endothermic event—shown in Fig. 4(b)—at around 900 °C suggests the occurrence of the reaction

$$2CoO + SnO_2 \overset{900^\circ C}{\rightarrow} Co_2SnO_4 \quad (8)$$

Thus, results from the thermal analyses together with the microstructure characterization by XRD and SEM suggest that reactions (7) and (8) occur nearly within the same temperature range, in such a way that once CoO is formed, it reacts with tin oxide to give rise to the spinel phase. This argument is supported by previous results reported by the same research group [16–19]. As observed in Table 2, showing results from phase quantification, the amount of spinel formed is in good agreement with the amount of Co_3O_4 used (see column 5, wt% in Table 2).

As regards its effect on grain size, it can be suggested that Co_2SnO_4 acts as an inhibitor to the growth of SnO_2 grains and that its influence is reflected in an increase in the breakdown electric field as Co_3O_4 content is augmented from 1 to 5 mol%. A possible explanation is offered as follows. The electrical behavior of varistors is governed by the presence of voltage barriers at the grain boundaries. For a given varistor system each voltage barrier is characterized by a specific value V_B. The reference voltage barrier's behavior is described by

$$E_B = n_1 V_B \quad (9)$$

where E_B is the breakdown electric field and V_B is the potential barrier per grain, and n_1 is the number of grains per unit length, calculated by

$$n_1 = \frac{L}{d} \quad (10)$$

Eq. (10) is developed considering that d is the thickness of a cylindrical sample and L is the mean grain size. If the content of Co_3O_4 increases, then the grain size decreases and produces an increase in the value of n_1, with the consequent increase in the magnitude of V_B. In the current work, it is postulated that

Table 2
Weighted profile value (R_{wp}), expected value (R_{exp}), profile value (R_P), goodness of fit value (χ^2) and lattice constant.

Sample		Phase present	Lattice parameter (Å)				wt (%)	R_{wp} (%)	R_{exp} (%)	R_p (%)	χ^2
Co_3O_4 (mol%)	Pressing (Mpa)		a	b	c	$\alpha=\beta=\gamma$ (deg)					
1	55	SnO_2	4.73	4.73	3.18	90	98.4	13.48	4.02	9.96	11.22
		Co_2SnO_4	8.63	8.63	8.63	90	1.6				
5	55	SnO_2	4.73	4.73	3.18	90	87	9.05	3.43	5.79	6.96
		Co_2SnO_4	8.65	8.65	8.65	90	13				
1	110	SnO_2	4.73	4.73	3.18	90	98.3	13.47	4.11	9.96	10.71
		Co_2SnO_4	8.63	8.63	8.63	90	1.7				
5	110	SnO_2	4.73	4.73	3.18	90	87.1	9.10	3.48	6.16	6.80
		Co_2SnO_4	8.65	8.65	8.65	90	12.9				
1	166	SnO_2	4.73	4.73	3.18	90	98.5	13.85	4.17	10.11	10.98
		Co_2SnO_4	8.63	8.63	8.63	90	1.5				
5	166	SnO_2	4.73	4.73	3.18	90	87.4	9.34	3.75	9.34	6.19
		Co_2SnO_4	8.65	8.65	8.65	90	12.6				

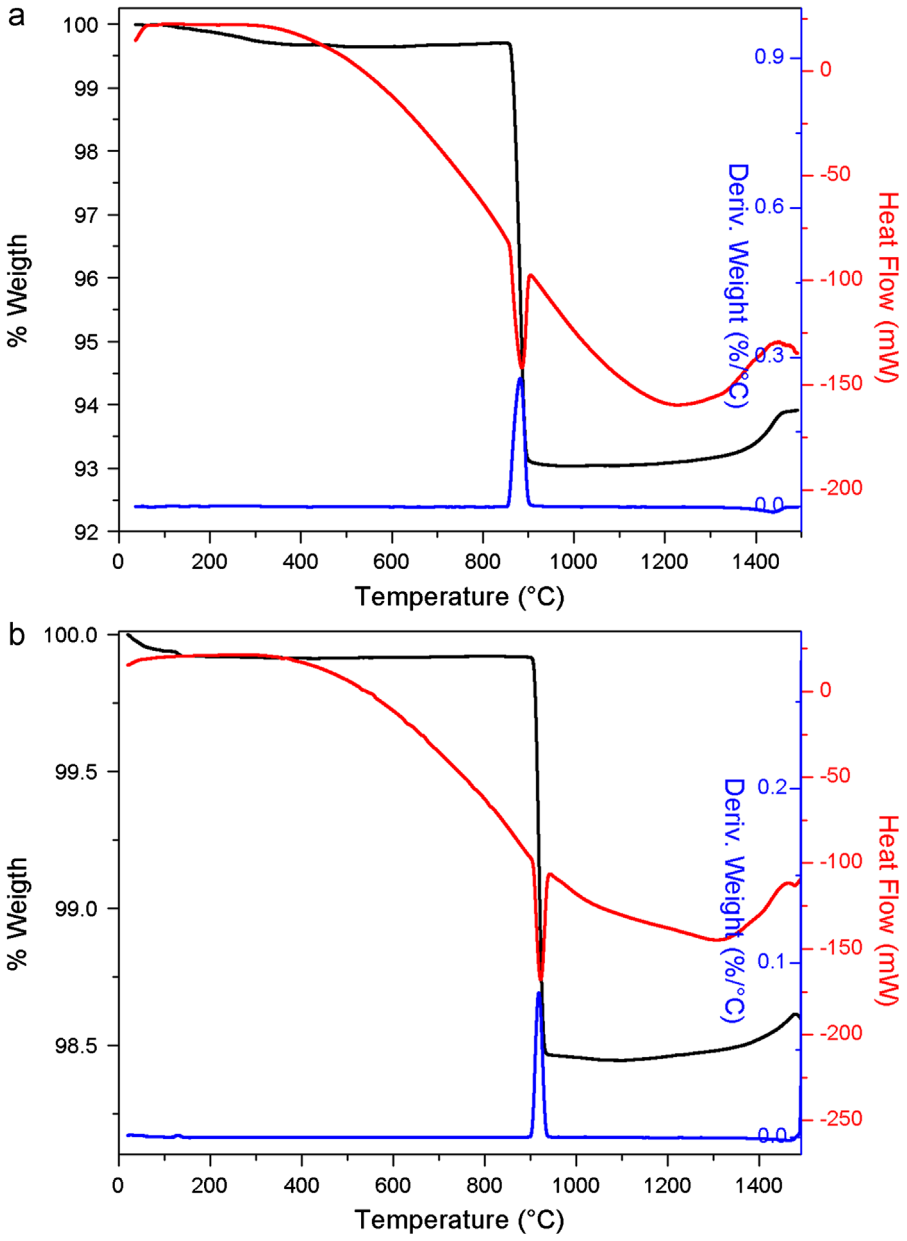

Fig. 4. TG–DTG–DSC curves of the decomposition for (a) Co_3O_4 and (b) stoichiometric amounts of Co_3O_4 and SnO_2.

this is the reason for the breakdown electric field increase with an increase in Co_3O_4 content. However, a question can be raised as to whether the effect of spinel can be achieved by adding that phase in an ex situ mode or whether it has to be formed in situ during processing, like in this case. In this regard, the authors are currently conducting a research to address this question.

4. Conclusions

In conclusion, the experimental results indicate that the nonlinearity coefficients (α) and breakdown electric fields (E_B) of the SnO_2–Sb_2O_5–Cr_2O_3 varistor system depend on the Co_3O_4 concentration and the compaction pressure. A low nonlinear coefficient of 9.5 for the varistor doped with 5 mol% Co_3O_4 and 55 MPa of compaction pressure were obtained. The best electrical characteristics were achieved at a compaction pressure of 166 MPa and 1 mol% Co_3O_4, that is, nonlinear coefficient of 13.24 and breakdown field of 830 V/cm. For the samples with 5 mol% Co_3O_4, either higher or lower of the compaction pressure results in decreasing nonlinear characteristics. The increase in the breakdown electrical field with increasing Co_3O_4 doping may be mainly attributed to the decrease of the grain size by formation of Co_2SnO_4 spinel-type phase. The decrease of the grain size is the origin for increasing threshold voltage. The varistor system of SnO_2–Sb_2O_5–Cr_2O_3 doped with Co_3O_4 is worthy of further investigation. A physical characterization by SEM of all the systems in order to evaluate densification will be carried out and published elsewhere.

Acknowledgments

Authors gratefully acknowledge Mr. Alberto Toxqui for assistance in the thermal characterization by TGA/DSC and Mr. Miguel Esneider for his valuable help in determining grain size of studied samples.

References

[1] L. Levinson, H. Philipp, ZnO varistors for transient protection, IEEE Transactions on Parts, Hybrids, and Packaging 13 (4) (1977) 338–343.
[2] M. Peiteado, Varistores cerámicos basados en óxido de cinc, Boletin de la Sociedad Espanola de Ceramica y Vidrio 44 (2) (2005) 77–87.
[3] Z.M. Jarzebski, J.P. Marton, Physical properties of SnO_2 materials: I. Preparation and defect structure, Journal of the Electrochemical Society 123 (7) (1976) 199C–205C.
[4] F. Gyger, M. Hübner, C. Feldmann, N. Barsan, U. Weimar, Nanoscale SnO_2 hollow spheres and their application as a gas-sensing material, Chemistry of Materials 22 (16) (2010) 4821–4827.
[5] Y. Shimizu, E. Di Bartolomeo, E. Traversa, G. Gusmano, T. Hyodo, K. Wada, M. Egashira, Effect of surface modification on NO_2 sensing properties of SnO_2 varistor-type sensors, Sensors and Actuators B: Chemical 60 (2–3) (1999) 118–124.
[6] S.A. Pianaro, P.R. Bueno, E. Longo, J.A. Varela, A new SnO_2-based varistor system, Journal of Materials Science Letters 14 (10) (1995) 692–694.
[7] Melo D. de, M.R.C. Santos, I.G. Santos, L.E.B. Soledade, M.I. B. Bernardi, E. Longo, A.G. Souza, Thermal and structural investigation of SnO_2/Sb_2O_3 obtained by the polymeric precursor method, Journal of Thermal Analysis and Calorimetry 87 (3) (2007) 697–701.
[8] J.A. Cerri, E.R. Leite, D. Gouvêa, E. Longo, J.A. Varela, Effect of Cobalt (II) oxide and manganese(IV) oxide on sintering of tin(IV) oxide, Journal of the American Ceramic Society 79 (3) (1996) 799–804.
[9] C. Li, J. Wang, W. Su, H. Chen, W. Zhong, P. Zhang, Effect of Mn^{2+} on the electrical nonlinearity of (Ni, Nb)-doped SnO_2 varistors, Ceramics International 27 (6) (2001) 655–659.
[10] C.P. Li, J.F. Wang, W.B. Su, H.C. Chen, W.X. Wang, G.Z. Zang, L. Xu, Nonlinear electrical properties of $SnO_2 \cdot Li_2O \cdot Ta_2O_5$ varistors, Ceramics International 28 (5) (2002) 521–526.
[11] C.-M. Wang, J.-F. Wang, C.-L. Wang, H.-C. Chen, W.-B. Su, G.-Z. Zang, P. Qi, Nonlinear electrical characteristics of SnO_2–CuO ceramics with different donors, Journal of Applied Physics 97 (12) (2005) 126103.
[12] J.A. Aguilar-Martínez, M.B. Hernández, A.B. Glot, M.I. Pech-Canul, Microstructure and electrical properties in SnO_2 ceramics with sequential addition of Co, Sb and Ca, Journal of Physics D: Applied Physics 40 (22) (2007) 7097.
[13] S.J. Park, K. Hirota, H. Yamamura, Densification of nonadditive SnO_2 by hot isostatic pressing, Ceramics International 11 (4) (1985) 158.
[14] P. Muné, E. Govea-Alcaide, R.F. Jardim, Influence of the compacting pressure on the dependence of the critical current with magnetic field in polycrystalline $(Bi–Pb)_2Sr_2Ca_2Cu_3O_x$ superconductors, Physica C: Superconductivity 384 (4) (2003) 491–500.
[15] N.F. Kunin, B.D. Yurchenko, Porosity versus pressure during the compacting of powders and probabilistic nature of densification law, Powder Metallurgy and Metal Ceramics 6 (12) (1967) 953–957.
[16] J.A. Aguilar-Martínez, A.B. Glot, A.V. Gaponov, M.B. Hernández, J. Guerrero-Paz, Current–voltage characteristics of SnO_2–Co_3O_4–Cr_2O_3–Sb_2O_5 ceramics, Journal of Physics D: Applied Physics 42 (20) (2009) 205401.
[17] J.A. Aguilar-Martínez, M.B. Hernández, M.I. Pech-Canul, A.B. Glot, J. Castillo-Torres, A comparative study between the mixed-oxide and high-energy milling planetary method on electrical and microstructural properties for a SnO_2-based ceramic system, Journal of Materials Processing Technology 209 (1) (2009) 318–323.
[18] J.A. Aguilar-Martínez, M.I. Pech-Canul, M. Esneider, A. Toxqui, S. Shaji, Synthesis, structure parameter and reaction pathway for spinel-type Co_2SnO_4, Materials Letters 78 (0) (2012) 28–31.
[19] J.A. Aguilar-Martínez, M.I. Pech Canul, M.B. Hernández, A.B. Glot, E. Rodríguez, L. García Ortiz, Effect of sintering temperature on the electric properties and microstructure of SnO_2–Co_3O_4–Sb_2O_5–Cr_2O_3 varistor ceramic, Ceramics International 39 (2013) 4407–4412.